Jurnal Integrasi
Vol. 18 No. 1, April 2026, 49-61
e-ISSN: 2548-9828

Article History
Received January 2026
Accepted April 2026

Implementation MPPT Using CUK Converter with Enhanced Harris Hawk Optimization Algorithm in Partial Shading Conditions

Muhammad Nizar Habibi[1], Faiz Rivaldi Fi'Adha[2], Rahmad Habibulloh[3], Dhea Ayu Nirmala Sari[4], Hasnira[5], Novie Ayub Windarko[6]

[12346]Politeknik Elektronika Negeri Surabaya, Jl. Raya ITS Sukolilo, Surabaya, 60111
[5]Politeknik Negeri Batam, Jl. Ahmad Yani, BatamKota, Batam 29461
Email: nizar@pens.ac.id

Abstract

Photovoltaic system efficiency drops significantly under Partial Shading Conditions (PSC) due to multi-modal power characteristics. Conventional algorithms and standard metaheuristics like Harris Hawks Optimization (HHO) frequently suffer from premature convergence and local peak entrapment. To resolve this, an Enhanced Harris Hawks Optimization (EHHO) strategy integrated with a continuous-current CUK converter is proposed for Maximum Power Point Tracking (MPPT). EHHO improves the search mechanism using logarithmic, exponential functions, and a traveling distance rate to significantly reduce the possibility of local optima entrapment. Simulations verify that EHHO delivers a superior average tracking accuracy of 99.43% within 0.260 s. In direct contrast, benchmark algorithms (PSO and HHO) exhibit severe performance degradation due to deceptive local peaks. Furthermore, EHHO yields the highest cumulative energy harvest of 27.44 Ws, confirming its robustness in maximizing energy extraction within dynamic environments.

Keywords: Photovoltaic, Partial Shading Conditions, CUK Converter, Maximum Power Point Tracking, Enhanced Harris Hawks Optimization.

1. Introduction

The increasing demand for electrical energy, together with growing environmental concerns and the depletion of fossil-fuel reserves, has accelerated the transition toward renewable energy resources. Among the available renewable technologies, photovoltaic (PV) systems have gained widespread acceptance because of their clean operation, modular structure, ease of installation, and continuously declining manufacturing costs. As a result, PV deployment has expanded significantly in residential, commercial, and utility-scale applications over recent years [1], [2].

Despite these advantages, the electrical output of PV modules is strongly influenced by environmental conditions. Variations in solar irradiance and cell temperature continuously alter the current–voltage and power–voltage characteristics of the array, causing the optimal operating point to shift over time. Consequently, extracting the maximum available energy from a PV system requires an effective Maximum Power Point Tracking (MPPT) mechanism capable of rapidly adapting to changing operating conditions [3], [4].

Traditional MPPT techniques, including Perturb and Observe (P&O) and Incremental Conductance (INC), remain popular because of their straightforward implementation and low computational requirements [5], [6]. However, their tracking capability deteriorates considerably under Partial Shading Conditions (PSC), where non-uniform irradiance creates multiple peaks on the P–V characteristic curve. In such circumstances, conventional methods frequently converge to a local maximum rather than the Global Maximum Power

Point (GMPP), resulting in reduced power extraction efficiency and degraded system performance [7], [8].

To overcome these limitations, numerous intelligent MPPT approaches have been developed. Data-driven methods such as Artificial Neural Networks (ANNs) have demonstrated the ability to model nonlinear PV behavior and estimate optimal operating points using historical information [9]. In addition, metaheuristic optimization techniques, including Particle Swarm Optimization (PSO), Genetic Algorithm (GA), Differential Evolution (DE), Artificial Bee Colony (ABC), Grey Wolf Optimization (GWO), Bat Algorithm (BA), and Cuckoo Search (CS), have been extensively investigated due to their capability to handle multimodal optimization landscapes commonly encountered under PSC [10]–[12]. Nevertheless, many of these methods still face challenges related to computational burden, convergence speed, susceptibility to local optima, and unstable tracking behavior under rapidly changing irradiance conditions [13].

Among various nature-inspired optimization methods, Harris Hawks Optimization (HHO) has emerged as a powerful metaheuristic due to its ability to emulate the cooperative predatory behavior of Harris hawks. The algorithm dynamically regulates global exploration and local exploitation processes, enabling efficient navigation of complex search spaces and effective identification of near-optimal solutions. Owing to these characteristics, HHO has been successfully employed in numerous nonlinear optimization problems and has demonstrated competitive performance in terms of convergence accuracy and computational efficiency [14].

The favorable search capability of HHO has motivated its adoption in renewable energy applications, particularly in Maximum Power Point Tracking (MPPT) for photovoltaic systems. Previous studies have shown that HHO-based MPPT approaches are capable of locating the Global Maximum Power Point (GMPP) under partial shading conditions with higher reliability than many conventional optimization techniques. The strong global search behavior of HHO allows it to avoid entrapment in local maxima, thereby enhancing the amount of energy harvested from photovoltaic arrays operating under non-uniform irradiance conditions [15], [16].

Despite these advantages, the original HHO formulation is not free from limitations. As the optimization process progresses toward the exploitation stage, the population may gradually lose diversity, reducing the algorithm's ability to explore alternative search regions. This issue can lead to premature convergence, oscillations around the optimum solution, and degraded tracking performance when environmental conditions vary rapidly [17]. Furthermore, an imbalance between exploration and exploitation may increase the likelihood of stagnation in local optima, limiting the robustness of the algorithm in practical MPPT implementations.

To overcome these drawbacks, several enhanced variants of HHO have been introduced in recent years. One notable improvement was proposed by Akl et al. through the Improved Harris Hawks Optimization (IHHO) algorithm, which incorporates modifications in both the exploration and exploitation mechanisms to strengthen population diversity and accelerate the search process. These enhancements enable the algorithm to achieve improved convergence characteristics and higher optimization accuracy, outperforming the conventional HHO algorithm as well as several contemporary metaheuristic optimization methods [18].

Although several enhanced versions of Harris Hawks Optimization (HHO) have been introduced in recent years, their utilization in photovoltaic maximum power point tracking applications is still relatively scarce, especially when combined with DC–DC converter topologies operating under partial shading conditions. Existing research has largely concentrated on improving the search and optimization capabilities of the algorithm, whereas its practical implementation in photovoltaic power conversion systems has received comparatively less attention. In addition, the impact of integrating an

enhanced HHO approach with a CUK converter on Global Maximum Power Point (GMPP) tracking performance under complex shading patterns has not been thoroughly explored. Recent literature has highlighted the growing need for intelligent MPPT strategies that can sustain high tracking precision and reliable operation under non-uniform irradiance conditions while simultaneously reducing convergence time and steady-state fluctuations [19], [20]. Motivated by these challenges, this work presents an MPPT scheme based on an Enhanced Harris Hawks Optimization (EHHO) algorithm coupled with a CUK converter for photovoltaic systems operating under partial shading conditions. The proposed method is designed to strengthen global search performance, accelerate convergence toward the GMPP, and improve tracking accuracy while mitigating power oscillations during steady-state operation. To validate its effectiveness, the proposed EHHO-based MPPT approach is assessed under several partial shading scenarios and benchmarked against existing MPPT techniques in terms of tracking performance and energy extraction capability.

2. Methodology and System Modeling

A. *PV System and Partial Shading Condition (PSC)*

A solar panel comprises interconnected solar cells designed to capture sunlight through positive and negative semiconductor layers, with each cell producing approximately 0.5–0.7 V. Photon impact releases electrons to establish a potential difference and continuous current, with the cell configuration directly influencing the overall output voltage and current. This behavior is represented by a single-diode equivalent circuit model incorporating series and parallel resistances.

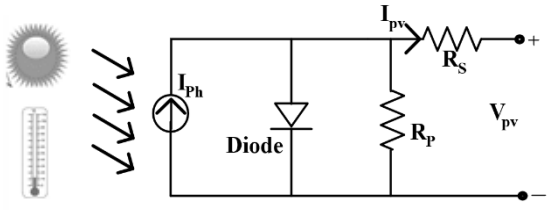

Figure 1: Equivalent Circuit Model of Photovoltaic Panel

Based on Figure 1, the equivalent mathematical model representing the output characteristics of the solar panel can be derived as follows:

$$I = I_{ph} - I_o\left(e^{\frac{(V+IR_S)q}{akT}} - 1\right) - \frac{(V+IR_S)}{R_{sh}} \quad (1)$$

Where:

- I : output current of the photovoltaic panel (A).
- I_{ph} : photogenerated current (A).
- I_o : diode reverse saturation current (A).
- V : output voltage of the photovoltaic panel (V).
- R_s : is the internal series resistance (ohm)
- R_{sh} : shunt (parallel) resistance (ohm)
- q : electron charge $1{,}6x10^{-19}$ (Coulomb).
- a : diode ideality factor.
- k : Boltzmann constant (Joule/Kelvin)
- T : absolute temperature of the cell (K).

Solar irradiance and ambient temperature fundamentally govern the photovoltaic (PV) panel's electrical behavior. Fluctuations in irradiance directly alter the characteristic curves; a decrease in light intensity causes a proportional drop in both the photogenerated current I_{ph} and total output power. Conversely, higher solar radiation maximizes the output current and drives the generated power closer to its peak capacity p_{max}.

Under Partial Shading Conditions (PSC), non-uniform irradiance creates an electrical mismatch across the photovoltaic (PV) array. Shaded cells experience a severe drop in short-circuit current I_{SC} , causing them to operate as loads rather than generators, which leads to destructive hot-spot formation. Although bypass diodes are integrated to mitigate these hot spots, their conduction alters the P-V characteristic curve, introducing a multi-peak profile that consists of a single Global Maximum Power Point (GMPP) and several Local Maximum Power Points (LMPPs). This non-linear behavior misleads conventional MPPT algorithms, trapping them at local optima and significantly reducing overall power extraction efficiency as illustrated in Figure 2.

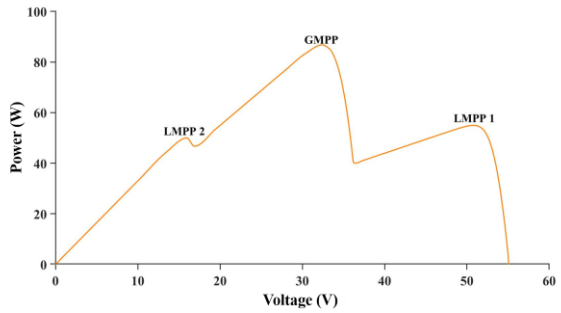

Figure 2: Output Power Characteristics of A Photovoltaic Array Under Partial Shading Conditions.

B. Modelling CUK Converter

A Cuk converter is an inverting buck–boost DC–DC converter capable of generating an output voltage whose polarity is reversed relative to the input source. Referring to Figure 3, the unique aspect of this circuit lies in its use of a coupling capacitor (c_1) as the primary medium for energy transfer unlike conventional converters that rely on inductors since the average inductor voltage during steady-state operation is zero.

The primary advantage of this topology is its completely continuous input and output current profiles. However, its main drawbacks include the necessity for large reactive components and the generation of high current stress across the switch, diode, and coupling capacitor.

The operational mechanism of the Cuk converter is generally analyzed based on two primary switching modes: when the switch is in the active or closed state (*switch on* atau t_{on}) and when the switch is in the inactive or open state (*switch off* atau t_{off}).

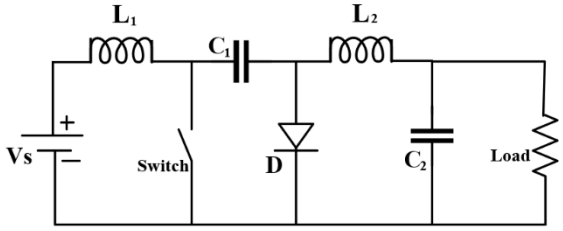

Figure 3: Cuk Converter Circuit Diagram

- **Switching Analysis Switch-On State (Closed Condition)**

When the switch is closed, the diode is reverse-biased, forcing the current to flow through the switch. In this mode, the input inductor (L_1) stores energy from the DC source as shown in Figure 4. Meanwhile, the output inductor (L_2) and filter capacitor (c_2) are energized by the discharge of the transfer capacitor c_1, with c_2 acting specifically to minimize voltage ripple at the load as shown in Figure 5.

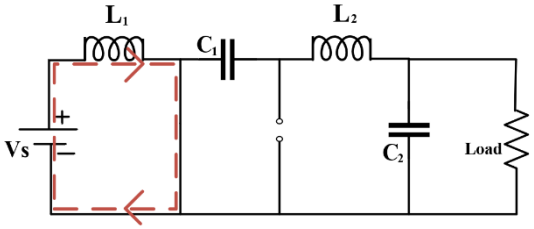

Figure 4: Cuk Converter during Switch-On: Left Loop Analysis

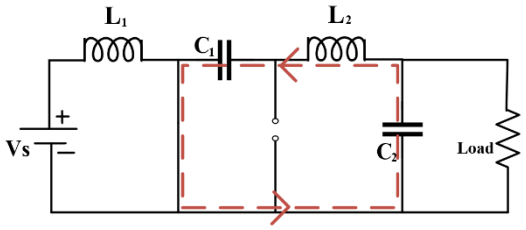

Figure 5: Cuk Converter during Switch-On: Right Loop Analysis

Evaluating the closed-loop circuit of the input stage during the switch-ON interval yields the following voltage relationship:

$$-V_s + V_{L_1(on)} = 0 \quad (2)$$

Simplification of this expression leads to:

$$V_{L_1(on)} = V_s \quad (3)$$

This equation implies that the voltage across inductor (L_1) equals the input DC source voltage under closed-switch conditions. Similarly, the right-loop analysis results in:

$$-V_{C_1} - V_o + V_{L_2(on)} = 0 \quad (4)$$

Rearranging this equation gives:

$$V_{L_2(on)} = V_{C_1} + V_o \quad (5)$$

Consequently, the voltage across inductor (L_2)during the ON-state represents the sum of the coupling capacitor voltage and the output load voltage.

- **Switching Analysis Switch-Off State (Open Condition)**

When the switch is open, the diode becomes forward-biased, allowing current to flow through it. In this phase, the coupling capacitor (c_1) charges from the DC source as shown in Figure 6. Simultaneously, in Figure 7, the output inductor (L_2) and filter capacitor (c_2) discharge their stored energy to supply

the load.

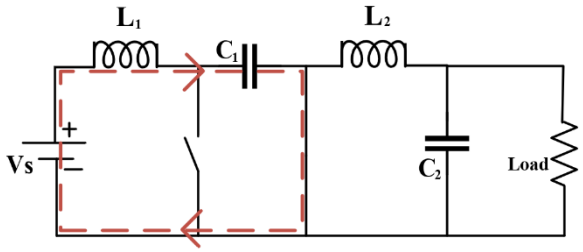

Figure 6: Cuk Converter during Switch-Off: Left Loop Analysis

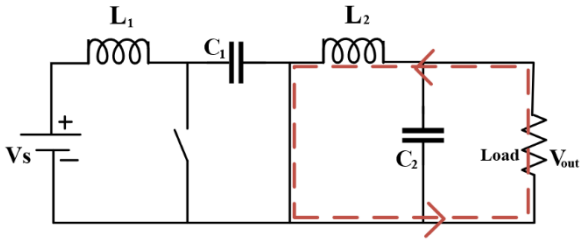

Figure 7: Cuk Converter during Switch-Off: Right Loop Analysis

On the other hand, analyzing the input loop during the switch-OFF interval establishes the following expression:

$$-V_s + V_{L_1(off)} + \mathrm{V_{C_1}} = 0 \quad (6)$$

Rearranging the variables yields:

$$V_{L_1(off)} = V_s - \mathrm{V_{C_1}} \quad (7)$$

Equation (6) demonstrates that the voltage across inductor ($\mathrm{L_1}$) during the open switching phase is determined by subtracting the transfer capacitor voltage from the input DC source. Meanwhile, the output loop analysis gives:

$$-V_o + \mathrm{V_{L_2(off)}} = 0 \quad (8)$$

Which can be simplified as:

$$\mathrm{V_{L_2(off)}} = V_o \quad (9)$$

This final condition indicates that the voltage across inductor ($\mathrm{L_2}$) during the switch-OFF state is equivalent to the output voltage but with an inverted polarity.

C. Harris Hawk Optimization (HHO) Algorithm

The Harris Hawks Optimization (HHO) algorithm is a metaheuristic approach inspired by the cooperative hunting behaviors of Harris hawks. It models their synchronized surprise attacks and dynamic chasing methods to find optimal solutions. The algorithm's execution is divided into three main phases: exploration, transition, and exploitation.

Phase 1: Exploration

In this preliminary phase, the hawks are randomly distributed across the search space, adjusting their positions based on the locations of other swarm members or the intended prey, formulated as:

$$\alpha = |X_{\mathrm{rand}}(t) - 2r_2 X(t)| \quad (10)$$

$$\beta = \left(LB + r_4(UB - LB)\right) \quad (11)$$

$$X(t+1) = \begin{cases} X_{rand(t)} - r_1 \cdot \alpha & q \geq 0.5 \\ \left(X_{rabbit} - X_{m(t)}\right) - r_3 \cdot \beta & q < 0.5 \end{cases} \quad (12)$$

$$X_m(t) = \frac{1}{N}\sum_{i=1}^{N} X_i(t) \quad (13)$$

Where $X(t+1)$ and $X(t)$ represent the position of the hawks in the next and current iteration, respectively. $X_{rabbit}(t)$ denotes the position of the prey (the best solution obtained so far), while $X_m(t)$ represents the average position of the current population. The variables r_1, r_2, r_3, r_4 and q are random numbers uniformly distributed between 0 and 1. UB and LB denote the upper and lower bounds of the search space, and N is the total number of hawks.

Phase 2: Transition from Exploration to Exploitation

During this phase, the transition between exploration and exploitation is dictated by the prey's escaping energy, which is modeled by the following equation:

$$E_1 = 2E_0\left(1 - \frac{t}{T}\right) \quad (14)$$

Where E represents the escaping energy of the prey, T is the maximum number of iterations, and E_0 is the initial state of the energy which randomly fluctuates between -1 and 1.

Phase 3: Exploitation

In the exploitation phase, a rapid strike accelerates the convergence rate. Furthermore, the algorithm employs four distinct pursuit strategies to model the prey's evasion tactics, which depend on the escape probability [r]. This probability dictates whether the evasion is successful or unsuccessful. The

specific besieging mechanism is controlled by the escaping energy parameter [E], where $|E| \geq 0.5$ activates a soft besiege and [E < 0.5] triggers a hard besiege approach.

1) Soft Besiege

In scenarios where $r \geq 0.5$ and $| E | \geq 0.5$, a soft besiege strategy is employed by the Harris hawks. During this maneuver, they slowly close in on the prey to gradually drain its escaping energy before launching a surprise strike. The corresponding position update is mathematically given by:

$$X(t+1) = \Delta X(t) - E|JX_{\text{rabbit}}(t) - X(t)| \quad (15)$$

$$X(t) = X_{\text{rabbit}}(t) - X(t) \quad (16)$$

Where $\Delta X(t)$ is the difference between the position of the rabbit and the current hawk, and J indicates the random jump strength of the prey during the escape process, determined by , $J = 2(1 - r_5)$, with r_5 being a random number inside (0,1).

2) Hard Besiege

In situations where $r \geq 0.5$ and $| E | < 0.5$, the prey's energy reserves are fully depleted, leaving it unable to escape. Therefore, the swarm directly performs a surprise pounce without any preliminary encircling phase. This positional update is mathematically formulated as:

$$X(t+1) = X_{\text{rabbit}}(t) - E|\Delta X(t)| \quad (17)$$

Under the conditions where $r < 0.5$ and $| E | \geq 0.5$, the swarm implements an adaptive ambush mechanism utilizing progressive rapid dives. This aggressive pursuit allows the hawks to fine-tune their positions in response to the prey's movement patterns, thereby maintaining an optimal balance between the exploration and exploitation stages. The candidate positions are evaluated using the following equations:

$$Y = X_{\text{rabbit}} - E|JX_{\text{rabbit}}(t) - X(t)| \quad (18)$$

$$Z = Y + S \times LF(D) \quad (19)$$

The Lévy flight can be defined as follows:

$$LF(d) = 0.01 \times \frac{u \times \sigma}{|v|^{1/\beta}} \quad (20)$$

$$\sigma = \left(\frac{\Gamma(1+\beta) \times sin(\frac{\pi\beta}{2})}{\Gamma(\frac{1+\beta}{2}) \times \beta \times 2^{(\frac{\beta-1}{2})}} \right)^{\frac{1}{\beta}} \quad (21)$$

Where D or dim is the dimension of the problem, u and v are random values between 0 and 1, and β is a default constant set to 1.5.

The candidate solution is updated via the following expression:

$$X(t+1) = \begin{cases} Y \text{ if } F(Y) < F(X(t)) \\ Z \text{ if } F(Z) < F(X(t)) \end{cases} \quad (22)$$

3) Hard Besiege with Progressive Rapid Dives

In scenarios where $r < 0.5$ and $| E < 0.5$, the escaping energy of the prey is completely exhausted. To capture the target, the hawks execute a hard besiege combined with a definitive surprise pounce. During this terminal stage, the population drastically reduces the spatial gap between the escaping prey and the swarm's average position. Therefore, the positional updates are mathematically dictated by:

$$X(t+1) = \begin{cases} Y \; if \; F(Y) < F(X(t)) \\ Z \; if \; F(Z) < F(X(t)) \end{cases} \quad (23)$$

The candidate positions are calculated as:

$$Y = X_{\text{rabbit}}(t) - E|JX_{\text{rabbit}}(t) - X_m(t)| \quad (24)$$

$$Z = Y + S \times LF(D) \quad (25)$$

D. Enhanced Harris Hawk Optimization (EHHO) Algorithm

Although the conventional Harris Hawks Optimization (HHO) algorithm possesses robust search capabilities, it frequently falls into local minima and sometimes fails to achieve an ideal balance between global exploration and local exploitation. Some of the besiege strategies in standard HHO are overly simple and tend to converge too quickly, causing the algorithm to miss search regions that potentially contain the true optimal solutions. To address these drawbacks, the Enhanced Harris Hawks Optimization (EHHO) proposes comprehensive enhancements in the exploration phase and three strategies within the exploitation phase.

1) Exploration Phase Update

In the exploration phase of standard HHO, the position update (perching) is based on random locations, which does not necessarily provide a well-distributed search. To avoid stagnation in suboptimal solutions, EHHO modifies this phase by utilizing the properties of logarithmic and exponential functions to generate new random values in previously unexplored

regions. This is mathematically formulated as follows:

$$X(t+1) = \begin{cases} X_m(t) * 0.5 - \begin{pmatrix} (X_{rand}(t) + r_1 * X(t)) \\ +(X_{rand}(t) + r_1 * X(t)) \end{pmatrix} & q \geq 0.5 \\ (X_{rabbit}(t) - X_m(t)) - r_3 \begin{pmatrix} LB \\ + r_4(UB - LB) \end{pmatrix} & q < 0.5 \end{cases} \quad (26)$$

Where r_1 is a probability variable updated using logarithmic and exponential functions to significantly accelerate the exploration rate:

$$r_1 = 1 - \log(1 + e^{ab}) \quad (27)$$

Where a and b are predefined constant parameters used to control the exponential growth rate.

2) Exploitation Phase Update

During the exploitation phase, EHHO optimizes the besiege strategies to accelerate the convergence rate and maintain solution diversity through the following three modifications:

In conventional HHO, the unnatural jumps of the prey (rabbit) as it attempts to escape are sometimes ignored. This stage is updated by incorporating a random jump probability variable of the prey (J_1) to allow the optimization process to find the global solution more precisely. The position update equation becomes:

$$X(t+1) = 0.01 \cdot E \cdot X_{rabbit}(t) - 0.1 \cdot |J_1 \cdot X_{rabbit}(t) - X_m(t)| \quad (28)$$

Where the random jump value is defined as $J_1 = 2 \cdot rand - 1$.

To rapidly increase the diversity of the existing population, the steps in Strategy 3 are replaced with a formulation inspired by the average traveling distance rate. This rate is controlled by the variable G_1:

$$G_1 = i \cdot \left(1 - \frac{\frac{1}{T_i}}{\frac{1}{T_i^{\bar{i}}}} \right) \quad (29)$$

The candidate positions (Y and Z) are evaluated using the following equations:

$$Y = \frac{X_{rabbit}(t)}{i} - rand \cdot E \cdot |G_1 \cdot J \cdot X_{rabbit}(t) - X(t)| \quad (30)$$

$$Z = X_{rabbit}(t) - rand \cdot E \cdot |G_1 \cdot J \cdot X_{rabbit}(t) - X(t)| - 1.5 \cdot G_2 \cdot Levy(dim) \quad (31)$$

Where G_2 is set as a constant ($G_2 = 6$). The final position of the hawks in the next iteration $X(t+1)$ is then selected based on the best fitness value between position (Y *and* Z). The update in this stage employs the average traveling distance rate approach to prevent the algorithm from slipping back into local optima and to accelerate the attainment of the optimal point. The difference is that this process centers around the average position of the entire population, $X_m(t)$.. The candidate solution equations become:

$$Y = \frac{X_{rabbit}(t)}{i} - rand \cdot E \cdot |G_1 \cdot J \cdot X_{rabbit}(t) - X_m(t)| \quad (32)$$

$$Z = X_{rabbit}(t) - rand \cdot E \cdot |G_1 \cdot J \cdot X_{rabbit}(t) - X_m(t)| - 1.5 \cdot G_2 \cdot Levy(dim) \quad (33)$$

The complete operational workflow of the proposed EHHO algorithm, incorporating the mathematical models into the closed-loop MPPT mechanism, is illustrated in Figure 8. This flowchart systematically delineates the step-by-step procedure, starting from the initial parameter configuration through to the final convergence of the optimal duty cycle. In addition, it highlights the interaction between the optimization process, fitness evaluation, and duty-cycle updating mechanism, providing a clearer understanding of how the EHHO algorithm guides the photovoltaic system toward the global maximum power point under varying operating conditions.

3. Experimental Results and Analysis

A. Performance Evaluation and Robustness of The Proposed EHHO Under Partial Shading

A comprehensive series of closed-loop simulations was conducted within the PSIM environment to validate the transient response and tracking capabilities of the proposed EHHO maximum power point tracking (MPPT) framework.

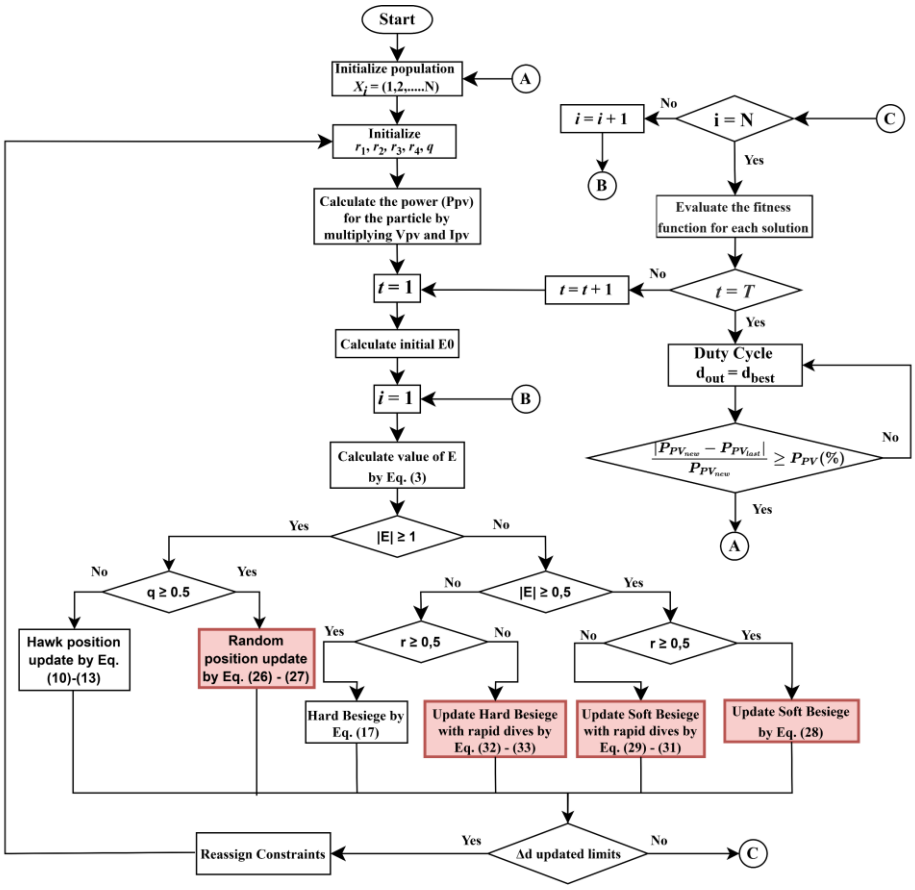

Figure 8: The Flowchart of Proposed EHHO-Based MPPT Method

TABLE I

CONTROL PARAMETERS OF THE EVALUATED ALGORITHMS

Method	Parameter Configuration
EHHO	Population size = 5, $\beta = 1.5, q = \text{rand}$
HHO	Population size = 5, $\beta = 1.5, q = \text{rand}$
PSO	Population size = 5, $\omega = 0.4, c_1 = 1.5, c_2 = 1.5$

To maintain an equitable comparative analysis, the population size for all evaluated optimization techniques was uniformly restricted to five search agents. The specific control parameters governing the operational mechanics of each algorithm are comprehensively outlined in Table I. Following the configurations established in Table I, the algorithms' robustness was tested across four distinct environmental setups.

These testing conditions incorporate a standard uniform irradiance profile alongside three challenging partial shading conditions (PSCs). Figure 9 illustrates the theoretical Power–Voltage (P–V) curves for each respective scenario, serving as fundamental references that pinpoint the exact spatial distribution of local and global peaks. These reference curves provide valuable insight into the complexity of the optimization landscape encountered by the MPPT algorithms, enabling a more comprehensive assessment of their capability to distinguish the global maximum power point from multiple local maxima under varying irradiance conditions. Establishing these theoretical baselines is critical to differentiate accurate global convergence from premature entrapment at suboptimal local maximum power points (LMPPs) caused by shading anomalies. To overcome the complexities of such multi-modal landscapes, the designed EHHO strategy is employed to secure a stable and highly accurate extraction of the

Global Maximum Power Point (GMPP).

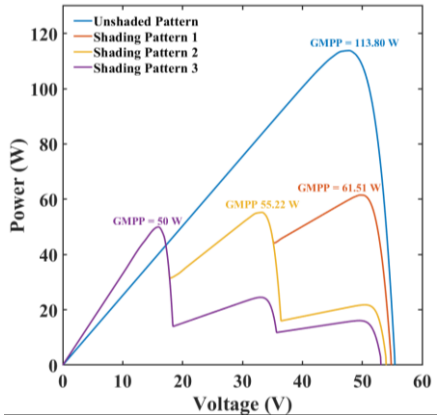

Figure 9. Power–Voltage (P–V) Characteristics of The PV Array Under Four Irradiance Scenarios Showing The Locations of The GMPP and Local Maxima, (a) Unshaded Pattern, (b) Shading Pattern 1, (c) Shading Pattern 2, and (d) Shading Pattern 3

The quantitative performance results obtained from the closed-loop MPPT simulations using the EHHO algorithm are summarized in Table II, including key tracking metrics under each operating scenario.

TABLE II

RESULTS OF MPPT CLOSED-LOOP SIMULATION BASED ON THE EHHO ALGORITHM

Condition	GMPP (W)	Power (W)	Time Tracking (s)	Accuracy (%)
Unshaded Pattern	113.80	113	0.26	99.26
Shading Pattern 1	61.51	61.48	0.259	99.95
Shading Pattern 2	55.22	54.53	0.261	98.75
Shading Pattern 3	50	49.87	0.258	99.74

These numerical results provide an initial assessment of the algorithm's effectiveness before a more detailed examination of its dynamic behavior. Subsequently, the actual dynamic responses and tracking trajectories of the EHHO method under these simulated atmospheric patterns are clearly visualized in Figure 10, enabling a comprehensive evaluation of its convergence characteristics and tracking performance.

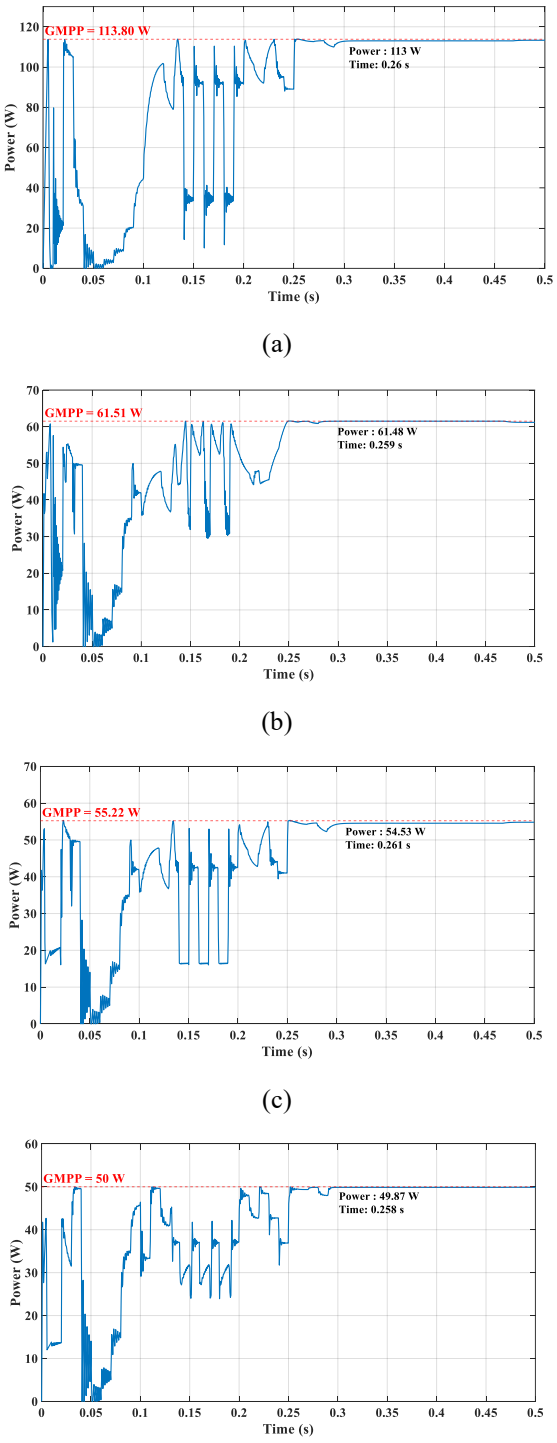

Figure 10. Dynamic Power-Tracking Responses of The EHHO Algorithm, (a) Unshaded Pattern, (b) Shading Pattern 1, (c) Shading Pattern 2, and (d) Shading Pattern 3

Table II summarizes the closed-loop MPPT performance of the proposed EHHO algorithm under uniform irradiance and partial shading conditions. The results show consistently high tracking accuracy of 99.26%, 99.95%, 98.75%, and 99.74%, with

convergence times ranging from only 0.258 s to 0.261 s. Moreover, the extracted power closely matches the theoretical GMPP in all scenarios, demonstrating the algorithm's ability to accurately identify the global optimum despite the presence of multiple local maxima.

Figure 10 demonstrates dynamic power-tracking responses of the EHHO algorithm, where the horizontal axis represents time (s) and the vertical axis represents output power (W). As observed in Figures 10(a)–(d), the EHHO algorithm initially performs an extensive exploration process, resulting in temporary power fluctuations before converging to the GMPP. Despite the increased complexity introduced by partial shading, the algorithm avoids LMPP entrapment and achieves stable convergence in all test cases. This performance is attributed to the enhanced exploration and exploitation mechanisms incorporated into EHHO, enabling reliable GMPP tracking with high accuracy and rapid convergence under varying irradiance conditions.

B. Comparative Evaluation of Steady-State Accuracy under Shading Patterns

This section systematically evaluates the tracking performance of the formulated EHHO strategy in juxtaposition with conventional optimization methods across unshaded and complex shading conditions.

TABLE III

MPPT TRACKING PERFORMANCE ACROSS VARIOUS SHADING PATTERNS

Condition	GMPP (W)	Method	Power (W)	Time (s)	Accuracy (%)
Unshaded Pattern	113.80	EHHO	113	0.26	99.26
		HHO	110.21	0.318	96.85
		PSO	109.71	0.360	96.40
Shading Pattern 1	61.51	EHHO	61.48	0.259	99.95
		HHO	58.66	0.320	95.37
		PSO	58.01	0.359	94.31
Shading Pattern 2	55.22	EHHO	54.53	0.261	98.75
		HHO	52.77	0.321	95.57
		PSO	50.80	0.362	92
Shading Pattern 3	50	EHHO	49.87	0.258	99.74
		HHO	47.58	0.319	95.15
		PSO	47.43	0.361	94.86

The quantitative performance indicators extracted from the tracking waveforms (depicted in Figure 11) are comprehensively compiled in Table III. This comparative tabulation provides a definitive benchmark to validate the superior convergence velocity and elevated tracking precision of the EHHO framework when navigating severe P-V curve nonlinearities.

The results presented in Table III and Figure 11 demonstrate the superior tracking performance of the proposed EHHO algorithm compared with conventional HHO and PSO methods.

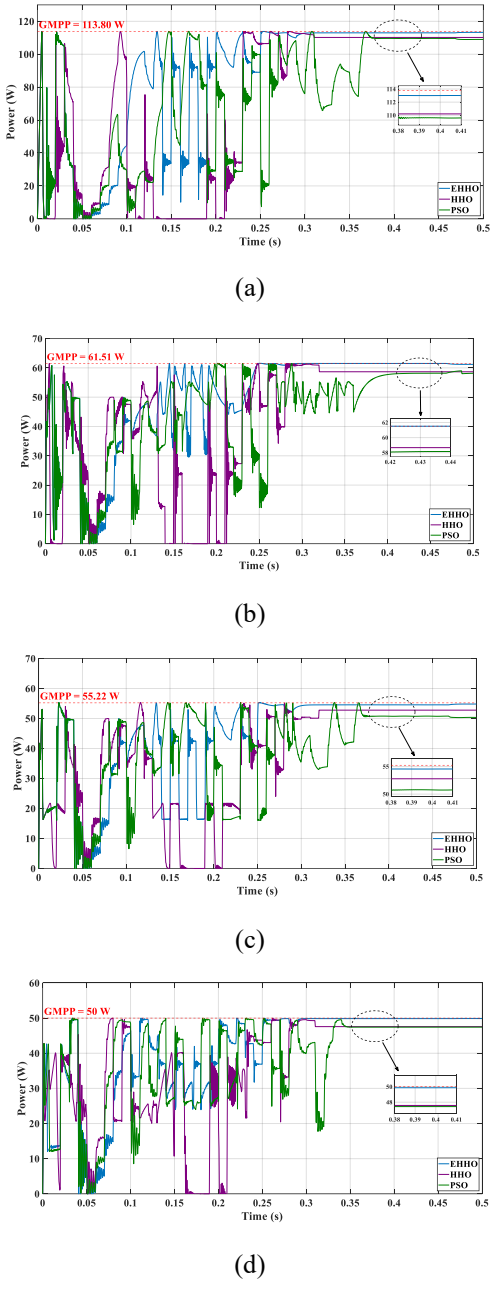

Figure 11. Comparative MPPT Tracking Trajectories Under: (a) Unshaded Pattern, (b) Shading Pattern 1, (c) Shading Pattern 2, and (d) Shading Pattern 3

Under unshaded conditions, EHHO achieves the highest extracted power of 113 W with 99.26% accuracy and the fastest convergence time of 0.260 s. As shown in Figure 11(a), EHHO reaches the GMPP more rapidly and exhibits a more stable trajectory than benchmark algorithms.

The performance advantage becomes more evident under partial shading conditions. In Shading Pattern 1, EHHO attains 99.95% accuracy, outperforming HHO (95.37%) and PSO (94.31%). Similarly, under the more complex Shading Pattern 2, EHHO maintains 98.75% accuracy, whereas HHO and PSO drop to 95.57% and 92.00%, respectively. Figure 11(b)–(c) shows that the conventional algorithms experience greater oscillations and are more susceptible to local peak entrapment. The larger oscillations exhibited by PSO suggest a slower stabilization process around the GMPP, resulting in lower tracking accuracy compared with EHHO. Similarly, the conventional HHO exhibits a higher tendency toward premature convergence, which may increase the likelihood of becoming trapped around local maximum power points. In contrast, the proposed EHHO preserves exploration capability through logarithmic–exponential position updating and traveling-distance-rate-based exploitation mechanisms. These enhancements improve the balance between exploration and exploitation, allowing the algorithm to locate the GMPP more consistently and achieve higher tracking accuracy under complex partial shading conditions. A similar trend is observed in Shading Pattern 3, where EHHO achieves 49.87 W with 99.74% accuracy and the shortest tracking time of 0.258 s. In contrast, HHO and PSO converge to lower steady-state power levels. Overall, EHHO delivers the highest average tracking accuracy of 99.43% and an average convergence time of approximately 0.260 s. These results confirm that the enhanced exploration and exploitation mechanisms effectively improve global search capability, prevent premature convergence, and ensure reliable GMPP extraction under challenging partial shading conditions. Although EHHO introduces additional mathematical operations through logarithmic and exponential functions, the population size remains limited to five search agents, thereby maintaining a computational burden suitable for real-time MPPT applications. This characteristic enables the proposed method to achieve improved tracking performance without significantly increasing computational complexity.

C. Evaluation of Total Energy

The final stage evaluates the energy extraction efficacy of the proposed EHHO strategy in comparison with the conventional HHO and PSO algorithms.

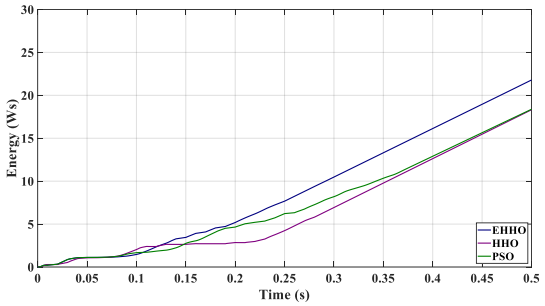

Figure 12. Comparison of Cumulative Energy Produced by Each MPPT Algorithm

This assessment monitors the system's operational response to rigorously verify overall transient stability during abrupt intensity shifts. As demonstrated in Figure 12, the EHHO framework exhibits superior adaptability, maintaining a highly consistent and accelerated energy accumulation trajectory compared to the baseline benchmarks. The steeper slope of the EHHO energy accumulation curve indicates that the algorithm spends less time operating away from the GMPP during transient periods. Consequently, more energy is harvested throughout the observation interval compared with HHO and PSO.

TABLE IV

SUMMARY OF CUMULATIVE ENERGY YIELD

Method	Total Energy Harvested (Ws)
EHHO	27.44
HHO	24.01
PSO	23.82

Based on the quantitative data consolidated in Table IV, the EHHO framework achieves the highest performance baseline with a total energy yield of

27.44 Ws. This targeted outcome confirms that the engineered EHHO architecture successfully minimizes severe power dissipation and significantly reduces settling times during volatile environmental fluctuations. Conversely, the traditional methods suffer from notable energy losses, with HHO and PSO underperforming at 24.01 Ws and 23.82 Ws, respectively. By fundamentally optimizing the equilibrium between the exploration and exploitation phases, the proposed method secures an improved energy recovery capability, demonstrating its effectiveness for photovoltaic applications.

4. Conclusions

This paper presents an Enhanced Harris Hawks Optimization (EHHO)-based MPPT strategy integrated with a CUK converter for photovoltaic systems operating under partial shading conditions. The proposed EHHO improves the conventional HHO through logarithmic and exponential exploration mechanisms, along with a traveling distance rate in the exploitation phase, enabling effective avoidance of premature convergence and local optimum entrapment. Simulation results confirm the superiority of the proposed approach, achieving an average tracking accuracy of 99.43% with a rapid convergence time of approximately 0.260 s across various shading scenarios. Compared with conventional HHO and PSO methods, EHHO consistently demonstrates higher tracking accuracy, faster convergence, and improved robustness against complex multi-peak P–V characteristics. Furthermore, the proposed method delivers the highest cumulative energy yield of 27.44 Ws, highlighting its capability to minimize power losses during transient operation. These findings establish the EHHO-CUK framework as an effective and reliable solution for high-performance photovoltaic energy harvesting under challenging environmental conditions. Although the proposed EHHO demonstrates excellent performance under PSIM-based simulations, practical implementation challenges such as sensor noise, converter losses, switching delays, and computational burden on embedded controllers have not yet been investigated. Therefore, future work will focus on hardware implementation and experimental validation under real photovoltaic operating conditions.

Acknowledgment

This research was supported by the Internal Research Grant of Politeknik Elektronika Negeri Surabaya (PENS) 2026 under contract number No. 012/SP2H/PENS/PPK/2026.

References

[1] M. Yılmaz, “Comparative Analysis of Hybrid Maximum Power Point Tracking Algorithms for Photovoltaic Systems Under Partial Shading Conditions,” Sustainability, vol. 16, no. 10, pp. 4199, 2024.

[2] D. Jia and D. Wang, “A Maximum Power Point Tracking Strategy Based on Harris Hawk Optimization Algorithm,” Actuators, vol. 13, no. 11, pp. 431, 2024.

[3] S. Motahhir, A. El Hammoumi, and A. El Ghzizal, “The most used MPPT algorithms: Review and suitable embedded implementation,” Journal of Cleaner Production, vol. 246, 2021.

[4] M. A. B. Siddique, D. Zhao, and A. U. Rehman, “Emerging maximum power point control algorithms for PV system: Review, challenges and future trends,” Electr. Eng., vol. 107, no. 8, pp. 9807–9839, 2025.

[5] M. N. Habibi, D. N. Prakoso, N. A. Windarko, and A. Tjahjono, “Perbaikan MPPT Incremental Conductance menggunakan ANN pada berbayang sebagian dengan hubungan paralel,” ELKOMIKA, vol. 8, no. 3, pp. 546–560, 2020.

[6] L. Bhukya and S. Nandiraju, “Enhanced Maximum Power Point Techniques for Solar Photovoltaic Systems under Partial Shading Conditions: A Review,” Algorithms, vol. 15, no. 10, 2022.

[7] R. Chaibi et al., “Photovoltaic System MPPT Under Partial Shading Using Advanced Intelligent Control,” Energy Reports, vol. 8, pp. 2022.

[8] A. Basalamah et al., “Comparing MPPT Algorithms for Improved Partial-Shaded PV Systems,” Journal of New Technology and Engineering, vol. 2023.

[9] M. N. Habibi, M. S. W. Jati, N. A. Windarko, and A. Tjahjono, “Maximum power point tracking menggunakan algoritma artificial neural network berbasis arus hubung singkat panel

surya," J. Rekayasa Elektrika, vol. 16, no. 2, pp. 57–64, Aug. 2020.
[10] A. del Rio, J. C. Hernández, and F. Jurado, "Particle Swarm Optimization-Based Control for Maximum Power Point Tracking in Photovoltaic Systems," Information, vol. 14, no. 10, p. 556, 2023.
[11] C. Gonzalez-Castano, C. Restrepo, S. Kouro, and J. Rodriguez, "MPPT Algorithm Based on Artificial Bee Colony for PV System", IEEE Access, vol. 9, pp. 43121–43133, 2021.
[12] S. Motahhir, A. Derouich, A. El Ghzizal, and A. El Fadili, "Enhanced energy output from a PV system under partial shading conditions using Grey Wolf Optimization-based MPPT," Energy Reports, vol. 8, pp. 754–764, 2022.
[13] T. Sutikno, N. A. Rahim, and M. A. M. Radzi, "A Review of Recent Advances in Metaheuristic Maximum Power Point Tracking Algorithms for Solar Photovoltaic Systems Under Partial-Shading Conditions," Indonesian Journal of Science and Technology, vol. 7, no. 3, pp. 463–490, 2022.
[14] A. A. Heidari et al., "Harris Hawks Optimization: Algorithm and Applications," Future Generation Computer Systems, vol. 97, pp. 849–872, 2019.
[15] M. Mansoor, A. F. Mirza, Q. Ling, and M. I. Javed, "Harris hawk optimization-based MPPT control for PV systems under partial shading conditions," J. Clean. Prod., vol. 274, Art. no. 122857, 2020.
[16] V. Gali, B. C. Babu, R. B. Mutluri, M. Gupta, and S. K. Gupta, "Experimental investigation of Harris Hawk optimization-based maximum power point tracking algorithm for photovoltaic system under partial shading conditions," Optim. Control Appl. Methods, vol. 44, no. 2, pp. 577–600, 2023.
[17] A. G. Hussien, D. Oliva, B. Houssein, H. Rezk, and M. M. Ewees, "Recent Advances in Harris Hawks Optimization: A Review and Future Directions," Electronics, vol. 11, no. 12, Art. no. 1919, 2022.
[18] D. T. Akl, M. M. Saafan, A. Y. Haikal, and E. M. El-Gendy, "IHHO: an improved Harris Hawks optimization algorithm for solving engineering problems," Neural Comput. Appl., vol. 36, no. 20, pp. 12185–12298, 2024.
[19] L. Bhukya and S. Nandiraju, "Enhanced Maximum Power Point Techniques for Solar Photovoltaic Systems under Partial Shading Conditions: A Review," Algorithms, vol. 15, no. 10, Art. no. 365, 2022.
[20] M. Y. Worku and M. A. Abido, "A Comprehensive Review of Recent Maximum Power Point Tracking Algorithms for Photovoltaic Systems," Sustainability, vol. 15, no. 14, Art. no. 11132, 2023.